Supplemental Material

Extreme Suppression of Antiferromagnetic Order and Critical Scaling in a Two-Dimensional Quantum Magnet

Wenshan Hong,[1,2] Lu Liu,[1] Chang Liu,[1,2] 2 Xiaoyan Ma,[1,2] Akihiro Koda,[3,4] Xin Li,[5] Jianming Song,[5] Wenyun Yang,[6] Peng Cheng,[7] Hongxia Zhang,[7] Wei Bao,[7,8] Xiaobai Ma,[9] Dongfeng Chen,[9] Kai Sun,[9] Wenan Guo,[10,11] Huiqian Luo,[1,12] Anders W. Sandvik,[13,1,*] and Shiliang Li,[1,2,12,†]

[1] *Beijing National Laboratory for Condensed Matter Physics, Institute of Physics, Chinese Academy of Sciences, Beijing 100190, China*
[2] *School of Physical Sciences, University of Chinese Academy of Sciences, Beijing 100190, China*
[3] *Institute of Materials Structure Science, High Energy Accelerator Research Organization (KEK-IMSS), 1-1 Oho, Tsukuba 305-0801, Japan*
[4] *Department of Materials Structure Science, Sokendai (The Graduate University for Advanced Studies), Tsukuba, Ibaraki, 305-0801, Japan*
[5] *Key Laboratory of Neutron Physics and Institute of Nuclear Physics and Chemistry, China Academy of Engineering Physics, Mianyang 621999, China*
[6] *State Key Laboratory for Mesoscopic Physics, School of Physics, Peking University, Beijing, 100871, China*
[7] *Department of Physics and Beijing Key Laboratory of Opto-electronic Functional Materials & Micro-nano Devices, Renmin University of China, Beijing 1 00872, China*
[8] *Department of Physics, City Univesity of Hong Kong, Kowloon, Hong Kong*
[9] *Department of Nuclear Physics, China Institute of Atomic Energy, Beijing, 102413, China*
[10] *Department of Physics, Beijing Normal University, Beijing 100875, China*
[11] *Beijing Computational Science Research Center, Beijing 100193, China*
[12] *Songshan Lake Materials Laboratory, Dongguan, Guangdong 523808, China*
[13] *Department of Physics, Boston University, 590 Commonwealth Avenue, Boston, Massachusetts 02215, USA*
[*] e-mail: sandvik@bu.edu, [†] slli@iphy.ac.cn

We provide additional experimental (Sec. 1), theoretical (Sec. 2), and Monte Carlo simulation (Sec. 3) results supporting the conclusions of the main paper. Additional μSR $A(t)$ data are presented in Sec. 1 A and the fitting procedures are explained. Neutron diffraction data in the columnar AFM state are presented in Sec. 1 B and in Sec. 1 C we explain how the cross-over temperature T^* was determined from the neutron data. In Sec. 2, we derive the scaling form of the μSR relaxation rate λ. In Sec. 3, we present additional Monte Carlo results for the classical 2D Heisenberg model with W-type impurities.

1. ADDITIONAL EXPERIMENTAL INFORMATION

Polycrystalline samples of $Sr_2CuTe_{1-x}W_xO_6$ were synthesized from stoichiometric mixtures of SrO, CuO, TeO_2, and WO_3 powders by the solid-state reaction method reported previously [25–27, 29]. The μSR experiments were performed at the S1 ARTEMIS spectrometer (Proposal No. 2018B0156), J-PARC, with the mini cryostat down to 4 K. The neutron-diffraction experiments were carried out at Bamboo (λ = 2.358 Å) and Xingzhi (λ = 2.7302 Å) triple-axis spectrometers, and at the PKU High-Intensity Powder Neutron Diffractometer (λ = 2.3 Å) at China Advanced Research Reactor (CARR), and the Kunpeng triple-axis spectrometer (λ = 2.7302 Å) at Key Laboratory of Neutron Physics and Institute of Nuclear Physics and Chemistry, China. Neutron speed velocity selectors were used before the monochromator with the Bamboo and Xingzhi spectrometers.

A. Raw μSR data

The time dependent asymmetry $A(t)$ from our μSR experiments for x = 0 and 1 are shown in Fig. S1. As discussed in the main text, the $x = 0$ sample [Fig. S1(a)] has long-rage Néel AFM order, while the $x = 1$ sample [Fig. S1(b)] has long-range columnar order. It is clear that the fits by Eq. (1) are not good at low temperatures. This is in contrast with the good fits at x = 0.05 and 0.1, as shown in Figs. 3(a) and 3(b).

The reason for the suboptimal fits at x = 0 and 1 is that, in the ordered states, we need multiple relaxation rates to describe the data, as shown in Ref. [28]. Here we test the following simpler function:

$$A(t) = A_0[f + (1-f)\exp(-\lambda t)]G_z(t) + A_{\rm BG}. \quad \text{(S1)}$$

Compared to the fitting function in the main text, the new function introduces a factor f to effectively account for a sec-

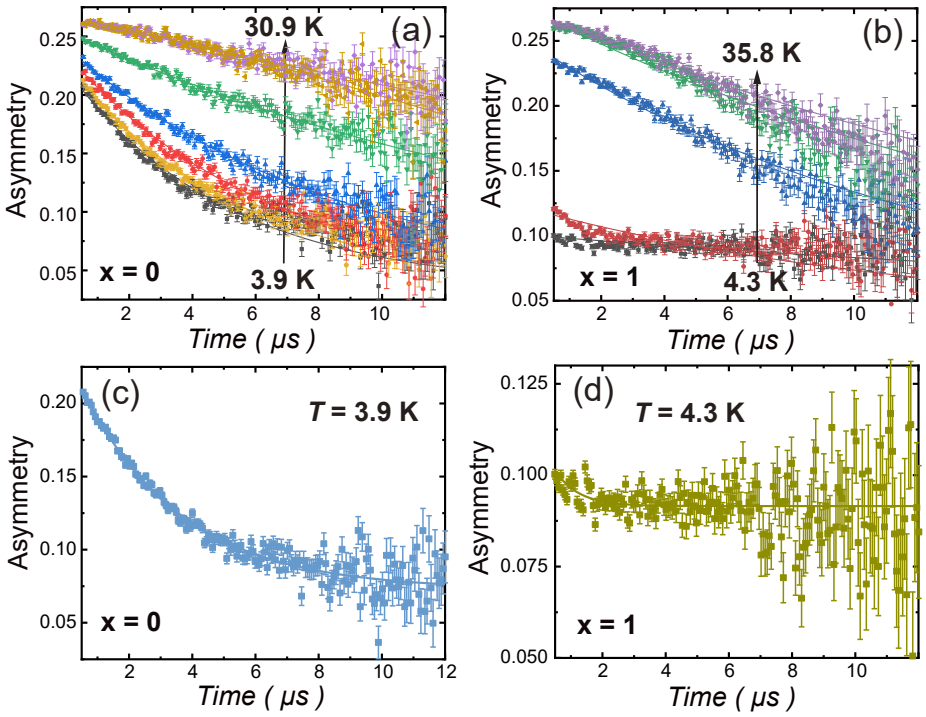

Figure S1. (a) and (b) show zero-field μSR spectra of $Sr_2CuTe_{1-x}W_xO_6$ samples with $x = 0$ and 1, respectively. Results for several temperatures are shown, witth the highest and lowest indicated for both samples. The curves are fits to the form Eq. (1) with a single relaxation rate. (c) and (d) show the spectra for $x = 0$ and 1, respectively, at the corresponding base temperatures. The curves are fits to the modified form Eq. (S1), which provides a better description of the data in the ordered state.

ond relaxation rate that is very small, so that its value is effectively zero on the time scale of the experiment. The very well fitted low-temperature results for x = 0 and 1 are shown in Figs. S1(c) and S1(d). It is worth noting that f is close to 1/3 for x = 0, and 1/2 for x = 1. We stress that we need the modified fitting form only for analyzing the ordered samples. As noted in the main text and shown in Figs. 3(a) and 3(b), for the short-range correlated samples with x = 0.05 and 0.1 the form Eq. (1) works essentially perfectly.

When fitting the μSR spectra, we have chosen a temperature-independent background $A_{\rm BG}$ = 0.035 for all the samples. This value is derived from the fact that the value of $A(t)$ at 1 μs at base temperature is about 1/3 of that above T_c, as shown in Ref. [28]. The same instrument was used for all the μSR measurements and all the samples have similar mass and were mounted in similar holders. For all these reasons we expect that the background should be close to the same for all the samples. Reasonable fits can be obtained for $A_{\rm BG}$ ranging from 0 to 0.1, and using different values in this range does not affect the conclusion of low-temperature power-law scaling $\lambda \sim T^{-\gamma}$ for x = 0.05 and 0.1; the exponent changes only marginally and $\gamma(0.1) > \gamma(0.05)$ always holds.

B. Neutron diffraction results for the columnar AFM state

Neutron diffraction data for x from 0.7 to 1 are shown in Fig. S2. At these W fractions the system is expected from previous studies [32] to have columnar AFM order at low temperature, which we confirm here with the resolution limited peaks at the corresponding wave-vectors.

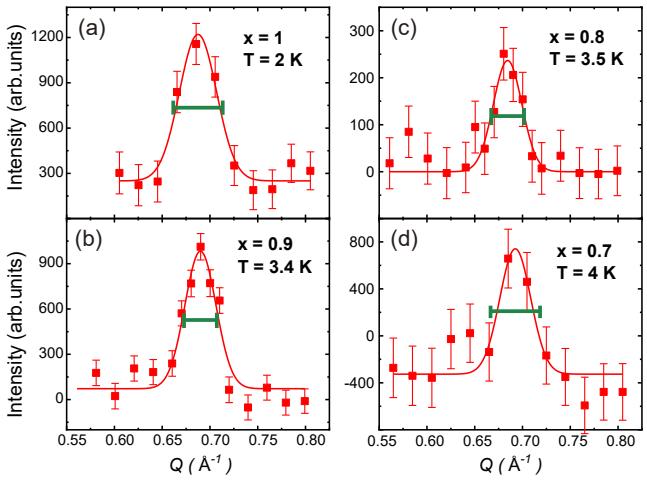

Figure S2. Neutron diffraction data along with Gaussian fits for x = 1 (a) 0.9 (b), 0.8 (c), and 0.7 (d). The peak locations correspond to $q = (0.5, 0, 0.5)$ and $(0, 0.5, 0.5)$, i.e., columnar AFM structure. The temperature is indicated in each panel and data taken at $T = 40$ K have been subtracted as background contributions. The green bars indicate the instrumental resolution.

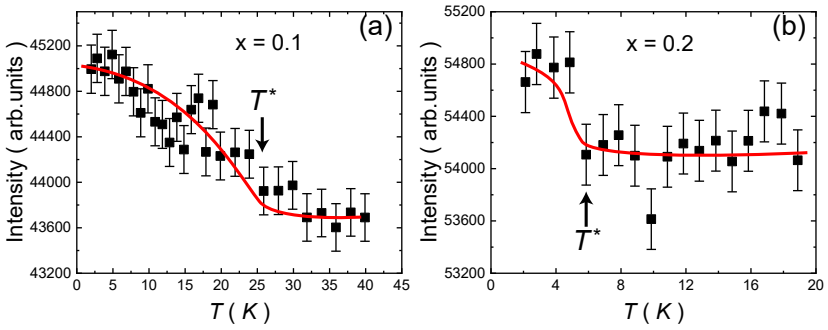

Figure S3. Temperature dependence of the magnetic peak intensity at $q = (0.5, 0.5, 0)$ in the sample with $x = 0.1$ in (a) and $x = 0.2$ in (b). The curves are guides to the eye and the cross-over temperature is defined as the point where the signal above background becomes significant, which implies errors of up to 3 K in these cases.

C. The cross-over temperature T^* from neutron diffraction

For the samples showing no phase transition into an ordered phase, in Fig. 4 we have indicated a temperature T^* where both the μSR and netron data show the onset of significant short-range correlations. It should be noted that, strictly speaking, T^* can not be defined unambiguously or uniquely as it merely signifies a sharp cross-over. Therefore, T^* determined from the neutron-diffraction measurements is not necessarily exactly equal to that from the μSR data, since these two techniques measure the system in different ways and with very different energy resolution. We here show that both experiments nevertheless produce compatible results for T^*.

Figures S3(a) and S3(b) show the temperature dependence of the magnetic peak intensity measured with neutron diffraction at wave-vector $q = (0.5, 0.5, 0)$ (corresponding to Néel AFM order) for the $x = 0.1$ and 0.2 samples, respectively. T^* is determined to be the temperature where a signal is detected above the high-T background, which is $T^* \approx 25$ and $T^* \approx 6$ K, respectively, for $x = 0.1$ and $x = 0.2$, with rather large error bars of 2-3 K due to the weak signal. Comparing with the μSR result for $x = 0.1$ in Fig. 4, the results agree well. We do not have μSR results for $x = 0.2$.

2. CRITICAL SCALING OF THE RELAXATION RATE

As discussed in the main paper, the $x = 0.05$ and 0.1 samples exhibit quantum-critical scaling in the μSR relaxation rate and are candidates for the RS state at low temperatures. According to QMC simulations of a "designer model" relizing the RS phase in a 2D quantum magnet [22, 23], this state is critical with large dynamic exponent, $z \geq 2$, with $z = 2$ at the transition from the Néel state and z increasing upon moving into the RS phase, and with dominant Néel type spin correlations decaying with distance r as r^{-2} universally. This correlation function formally implies that the exponent η in the standard form [36] of the quantum-critical correlation function for a system in d space dimensions,

$$C(r) \propto r^{-(d+z-2+\eta)}, \tag{S2}$$

depends on z through the relationship $\eta = 2 - z$. Thus, in the RS state this exponent is negative, which is normally not possible in uniform systems but is not uncommon in disordered systems.

The exponent η appears also in dynamical scaling forms, e.g., the NMR relaxation rate $1/T_1$ scales as T^η at the O(3) quantum-critical point in uniform antiferromagnets, where $z = 1$ [37]. One can expect the μSR relaxation rate λ, which like $1/T_1$ depends on local low-energy spin fluctuations, to scale in the same way. However, since the dynamic exponent $z \neq 1$ in the RS state, the T^η form has to be modified as follows: The correlation length in a quantum-critical system scales as $\xi \propto T^{-1/z}$, and we can therefore formally express the temperature as $T \propto \xi^{-z}$. For $z = 1$, we can write $\lambda \propto T^\eta \propto \xi^{-\eta}$, and the generalization to $z \neq 1$ is obtained by inserting the correct T-dependent expression for the correlation length. Thus, $\lambda \propto \xi^{-\eta} \propto T^{\eta/z}$. Using the form $\eta = 2-z$ in the RS state, we expect $\lambda \propto T^{-\gamma}$, where we have defined the positive exponent $\gamma = 1 - 2/z$, with $z \geq 2$. This is the exponent that was extracted from the data fits in Fig. 3(d).

The asymptotic scaling form of $\lambda(T)$ can also be derived in a more transparent way: First, consider the well known NMR spin-lattice relaxation rate $1/T_1$, which for a spin-isotropic system is given by [55]

$$\frac{1}{T_1} = \frac{\gamma^2}{2} \sum_{\mathbf{q}} A^2(\mathbf{q}) S(\mathbf{q}, \omega_{\mathrm{N}}), \tag{S3}$$

where γ is the gyromagnetic ratio, A_q is the Fourier transform of the hyperfine constants describing the coupling between the nuclear and electronic spins, and ω_{N} is the field-dependent nuclear resonance frequency. The hyperfine coupling is short-ranged in space, and if the nucleus considered is in the ion hosting the localized electronic spins (e.g., Cu NMR in the material considered here), it is often sufficient to consider purely local on-site interactions A_0, so that the momentum sum in Eq. (S3) reduces to $A_0^2 S_0(\omega_{\mathrm{N}})$, where $S_0(\omega)$ is the on-site (single-spin) dynamic structure factor.

Typically, the resonance frequency is much lower than other energy scales in the system, and the zero-frequency limit can be considered (unless there are significant spin diffusion contributions, which can cause low-frequency divergencies).

Thus, with these simplifications, which are often completely valid, the relaxation rate is proportional to $S_0(\omega \to 0)$ (with prefactors that are known or can be measured). Since μSR also is a probe of low-frequency local spin fluctuations, we expect the same form;

$$\lambda \propto S_0(\omega \to 0). \tag{S4}$$

The local dynamic spin structure factor $S_0(\omega)$ (and also its q dependent variant) can be calculated in various analytical approximative schemes or numerically; for example, it was calculated in the case of the 1D RS state in Ref. 56. However, the low-frequency limit is often challenging, especially in QMC calculations, where the corresponding imaginary-time dependent spin correlation function $G_0(\tau)$ has to be calculated and analytically continued to real frequency. To circumvent the latter step, Randeria et al. suggested a very useful approximation [57], which was expressed in a slightly different form in Ref. 56. Neglecting unimportant factors, the approximation amounts to

$$S_0(\omega \to 0) \propto \frac{1}{T} G_0(\tau = \beta/2), \tag{S5}$$

and then the relaxation rate Eq. (S4) is approximated as

$$\lambda \propto \frac{1}{T} G_0(\tau = \beta/2), \tag{S6}$$

where $\beta = 1/T$. Here we will use this form, which is expected in general to become better with decreasing T, to derive the critical scaling behavior of λ in the RS phase.

As already mentioned above, a quantum-critical spatial correlation function is conventionally written as Eq. (S2), where $d = 2$ in our case. The on-site correlation in imaginary time is modified by the dynamic exponent [36]

$$G_0(\tau) \propto \tau^{-(d+z-2+\eta)/z}, \tag{S7}$$

reflecting that space and (imaginary) time distances are related as $\tau \sim r^z$, which is used to obtain Eq. (S7) from Eq. (S2). Thus, in the RS state with the staggered spatial spin correlation function $C(r) \propto r^{-2}$, the time correlations take the form $G_0(\tau) \propto \tau^{-2/z}$. Using this form in Eq. (S6) immediately gives the scaling form $\lambda \propto T^{-(1-2/z)}$, in agreement with the result presented earlier. The fact that we observe this kind of scaling with $z > 2$, Fig. 3(d), with z also increasing upon moving further away from the Néel phase as predicted [22], constitutes strong support for an RS phase in $Sr_2CuTe_{1-x}W_xO_6$.

3. 2D HEISENBERG MODEL

For the Monte Carlo simulations of the classical Heisenberg models, we used methods that have been previously explained in detail in the literature [46, 47]. The simulations combine heat-bath sweeps with energy conserving "over-relaxation" updates. We found the latter to be particularly important for reaching the ground state of systems with a small number of W-type impurities. In all simulations, we started at a high temperature and gradually lowered the temperature in order to alleviate problems with long autocorrelation times. For the systems with more than one W impurity (random mixes of Te and W plaquettes) disorder averages were taken over hundreds of realizations of random locations of the impurities.

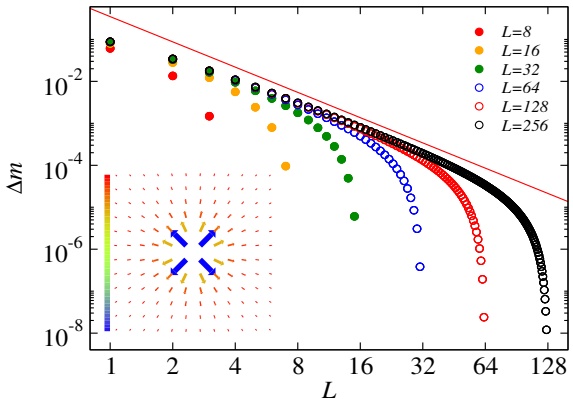

Figure S4. Plaquette impurity induced deformation of the Néel order parameter for different system sizes, as in Fig. 5 but with $J_2' = 0$.

In Fig. 5 in the main text we demonstrated an impurity induced deformation of the sublattice magnetization that decays with the distance r from the impurity as $1/r^2$. This decay implies that the total response of a single impurity diverges logarithmically with increasing system size. We here provide additional results demonstrating that the order parameter indeed vanishes for any concentration $x > 0$ of the impurities.

In the main paper, the Monte Carlo simulations were carried out with parameters approximating those estimated [33] for $Sr_2CuTe_{1-x}W_xO_6$. The bulk parameters for $x = 0$, illustrated in Fig. 1(a), were $J_1 = 1$ and $J_2' = 0.1$. Even with the small frustrating J_2' terms, the $T = 0$ order parameter is the fully colinear Néel state, and we do not expect that the frustration is in any way required to obtain the r^{-2} decay of the deformation. To explicitly demonstrate that the classical Heisenberg model with only the first-neighbor couplings J_1 also has the same impurity response as in Fig. 5, here in Fig. S4 we show simulation results for $J_2' = 0$. These results confirm that the r^{-2} form emerges as the system size increases.

The $1/r^2$ form with no angular dependence of the deformation of the order parameter may appear surprising in light of there being no such momopole-like solution of the Poisson equation, which provides the long-distance continuum description of the Néel state with impurities [58]. As will be discussed in more detail elsewehere [59], the plaquette impurity considered here can be regarded as a composite of two dipoles, with the relative angle of the deformation vectors in the xy plane chosen to minimize the energy. The angular degree of freedom of the deformation is missing in treatments of impurities in long-range ordered systems of spins with only two components [60].

For the following results we go back to $J_2' = 0.1$, and we expect the same kinds of behaviors also for $J_2' = 0$. In Fig. S5(a) we show results for the disorder-averaged $T = 0$

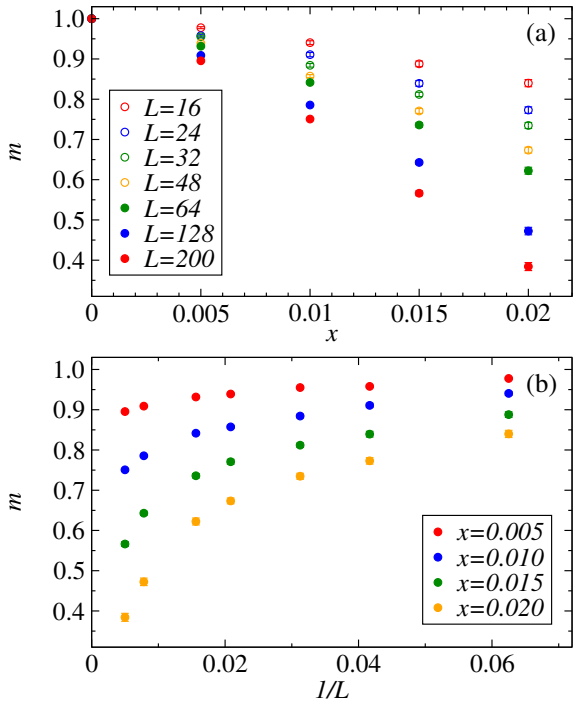

Figure S5. (a) Disorder averaged order parameter versus the concentration of W-type plaquette impurities, graphed for several system sizes. (b) Order parameter at several fixed impurity concentrations x graphed vs the inverse system size.

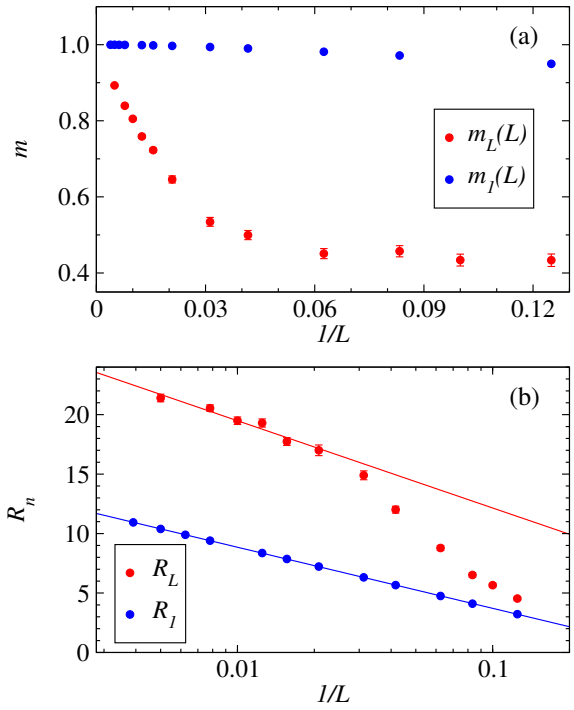

Figure S6. (a) Néel order parameter vs inverse system size in systems with a single impurity (blue symbols) and with L impurities (red symbols), graphed versus the inverse of the system size L. (b) Slope graphed on a log-linear plot of the magnetization curve at $x = 0$ based on the size-dependent definitions, Eqs. (S9) and (S10), with the data in (a). The lines are fits corresponding to the logarithmically divergent forms $R_n(L) \sim a_n + b_n \log(L)$ with both definitions (with systems containing $n = 1$ and $n = L$ impurities).

Néel order parameter m versus the concentration of impurities. Increasing the system size consistently leads to a smaller value of m. In Fig. S5(b) we show results versus the inverse system size for several low impurity concentrations. Here we can observe that m always decreases with increasing L. Given the logarithmic singularity suggested by the single-impurity response, the most natural scenario is that m vanishes in the thermodynamic limit for all $x > 0$, but it is difficult to demonstrate that reliably using results such as those in Fig. S5, because of the logarithmic-type singularity that makes extrapolations difficult.

A better way to investigate the presence or absence of order for small x, introduced in Ref. 5, is to consider a system with a single impurity to have concentration $x = 1/L^2$, and to compute the initial slope,

$$R = \frac{dm}{dx}, \tag{S8}$$

of the order parameter vs x based on this value;

$$R_1(L) = L^2[1 - m_1(L)], \tag{S9}$$

where m_1 is the value of m computed with the single impurity (averaged over the entire system). Then, if indeed $m = 0$ for $L \to \infty$ at $x = 0^+$, the slope $R_1(L)$ will diverge. In order to take into account possible subtle interaction effects, we here additionally use a modified approach with L randomly placed impurities in the L^2 system, for which the concentration is $x = 1/L$ and the slope is

$$R_L(L) = L[1 - m_L(L)], \tag{S10}$$

where $m_L(L)$ is the impurity-averaged order parameter for L impurities in the lattice with L^2 spins.

In Fig. S6(a) we show $m_1(L)$ and $m_L(L)$ versus $1/L$. In the former, we can see clearly the expected approach to the fully saturated bulk order parameter $m = 1$ when L increases. For $m_L(L)$ we also have to asymptotically approach the same limit, and this appears plausible though the convergence is slower, as expected, because of the higher concentration x for a given system size. In Fig. S6(a) we graph the initial slopes defined in Eqs. (S9) and (S10). Both quantities diverge logarithmically, confirming that the impurity response in the $x \to 0$ limit has a logarithmic singularity. Any other interpretation than $m(x) = 0$ for all $x > 0$ is then unlikely, as indicated also by the results in Fig. S6 for small but finite impurity concentrations.

The Néel order suppression for any $x > 0$ is also supported by the strong sensitivity of $T_c(x)$ to the 3D coupling $J_\perp$ in Fig. 4(b), which suggests that the transition into the ordered phase at $x > 0$ and $T > 0$ is due to the inter-layer effect. It would be intersting to also study the deformation induced by a single-impurity in the 3D coupled-layer system, but we have not yet done so. We should expect the $1/r^2$ decay to be cut off at some distance depending on $J_\perp$ (diverging as $J_\perp/J_1 \to 0$) and, therefore, the slopes defined in Eqs. (S9) and (S10) to be finite for any $J_\perp > 0$.

Related issues were recently discussed by Dey et al. in the context of a host system (the Heisenberg model on the triangular lattice) with coplanar AFM order [8]. While previous works have considered distruction of long-range order by dipolar impurities in two-component spin systems (the XY model) [60], this system lacks the rotational degree of freedom of the distortion field of impurities in the Heisenberg case. The lack of previous works on the plaquette impurity (which, as we pointed out, can be regarded as a composite of two dipoles at a certain relative angle) likely reflects the absence of experimental motivation before the investigations of $Sr_2CuTe_{1-x}W_xO_6$ demonstrated these particular coupling patterns [30–33].